PTEP

Prog. Theor. Exp. Phys. **2022** 113D01(11 pages)
DOI: 10.1093/ptep/ptac145

Cluster formation in neutron-rich Be and B isotopes

Hideaki Motoki[1,⋆], Yoshiki Suzuki[2], Tsuyoshi Kawai[1], and Masaaki Kimura[1,3,4]

[1] *Department of Physics, Hokkaido University, Sapporo 060-0810, Japan*
[2] *Research Center for Nuclear Physics (RCNP), Osaka University, Ibaraki 567-0047, Japan*
[3] *Nuclear Reaction Data Centre (JCPRG), Hokkaido University, Sapporo 060-0810, Japan*
[4] *RIKEN Nishina Center, Wako, Saitama 351-0198, Japan*
⋆E-mail: motoki@nucl.sci.hokudai.ac.jp

Received August 23, 2022; Accepted November 2, 2022; Published November 4, 2022

Evaluating the formation of clusters in finite and infinite nuclear systems is a fundamental problem in nuclear physics, and the variation in clustering in the isotope chain up to the neutron drip-line is one such intriguing phenomenon. Recently, experiments performed using the (p, $p\alpha$) reactions have revealed a negative correlation between α-cluster formation and neutron number in Sn isotopes, showing a trend opposite to that theoretically predicted for Be and B isotopes. Although the observed charge radii of the Be and B isotopes suggest the formation of clusters as the neutron drip-line is approached, these radii themselves are not a physical quantity that can directly probe the cluster structure. Here, we directly investigate the cluster formation in Be and B isotopes to elucidate the possibility of clustering as the neutron drip-line is approached. It has been shown that the sum of the S-factors (i.e., $S(\alpha)$, $S(^6\mathrm{He})$, and $S(^8\mathrm{He})$) increases as the neutron drip-line approaches, in agreement with those of previous studies. The results indicate that the excess neutrons contribute to the formation of ^{6}He and ^{8}He clusters as well as α clusters. Thus, $S(\alpha)$ is not sufficient to estimate the enhancement of clustering in Be and B isotopes.

Subject Index D10, D12, D13

1. Introduction

Cluster formation is a universal phenomenon exhibited at all levels constituting the hierarchy of matter. In the sub-atomic regime, the α-cluster structure plays an important role in both finite and infinite nuclear systems. In dilute nuclear matter, the formation of α clusters is theoretically predicted to depend on the nuclear density as well as the symmetry energy [1–4]. Notably, in finite nuclei, cluster formation is expected to be hindered by the growth of a neutron skin [5]. Therefore, it is important to clarify the correlation between the neutron-skin thickness and the cluster formation. Recently, it was shown that the proton-induced α knockout reaction (p, $p\alpha$) is useful for assessing the α-cluster formation at the nuclear surface [6]. Using this reaction, the negative correlation between the neutron-skin thickness and the α-cluster formation at the nuclear surface of Sn isotopes has been reported [7]. A similar negative correlation was also theoretically shown in neutron-rich C isotopes [8].

In contrast to the trend observed in Sn isotopes, the α-cluster formation in light nuclei, such as Be and B isotopes, is predicted to enhance as the neutron drip-line approaches [9–12]. The enhancement of the α-cluster formation in Be isotopes as the neutron drip-line is approached is theoretically well explained by the molecular orbital model, which assumes that the excess neutrons bond with two α particles, similar to the covalent electrons in a molecule [13–15]. For

© The Author(s) 2022. Published by Oxford University Press on behalf of the Physical Society of Japan. This is an Open Access article distributed under the terms of the Creative Commons Attribution License (https://creativecommons.org/licenses/by/4.0/), which permits unrestricted reuse, distribution, and reproduction in any medium, provided the original work is properly cited.

Downloaded from https://academic.oup.com/ptep/article/2022/11/113D01/6798384 by DESY-Zentralbibliothek user on 26 December 2022

example, in ^{12}Be, the two excess neutrons are promoted into the *sd*-shell across an $N = 8$ shell gap and enhance the clustering compared with that in ^{10}Be. The observed increase in the charge radii of the Be and B isotopes suggests the development of clusters as the neutron drip-line is approached [16–18].

However, direct observation of the enhancement in the clustering is a significant challenge. Therefore, a study based on the physical quantities that can directly probe the cluster structure is highly desirable. Consequently, we investigate the cluster formation probability, which can be experimentally measured via $(p, p\alpha)$ reactions, at the nuclear surfaces of Be and B isotopes through antisymmetrized molecular dynamics (AMD) calculations. We focus on the ^{6}He and ^{8}He clusters that are expected to emerge because of the excess neutrons near the neutron drip-line as well as the α clusters.

This paper is organized as follows. In Sect. 2, the theoretical framework of AMD is briefly explained. In Sect. 3, we present the numerical results and discuss the clustering in Be and B isotopes. Finally, Sect. 4 summarizes this work.

2. Theoretical framework

2.1. *Hamiltonian and model wave functions*

The microscopic Hamiltonian for an A-body system is expressed as

$$\hat{H} = \sum_{i}^{A} \hat{t}_i - \hat{t}_{\mathrm{c.m.}} + \sum_{i<j}^{A} \hat{v}_{ij}^{\mathrm{NN}} + \sum_{i<j\in\mathrm{proton}}^{A} \hat{v}_{ij}^{\mathrm{C}}, \tag{1}$$

where $\hat{t}_i$ and $\hat{t}_{\mathrm{c.m.}}$ denote the nucleon and center-of-mass kinetic energies, respectively. The Gogny D1S parameter set [19] is employed to represent the effective nucleon–nucleon interaction $\hat{v}_{ij}^{\mathrm{NN}}$, and the Coulomb interaction $\hat{v}_{ij}^{\mathrm{C}}$ is approximated by a sum of seven Gaussians.

The model wave function of the A-body system is a parity-projected Slater determinant,

$$\Phi^{\pi} = \hat{P}^{\pi} \mathcal{A}\{\phi_1 \phi_2 \cdots \phi_A\}, \tag{2}$$

where $\hat{P}^{\pi}$ denotes the parity projection operator and ϕ_i is the ith nucleon wave packet expressed by the deformed Gaussian [20]:

$$\phi_i(\boldsymbol{r}) = \exp\left\{-\sum_{\sigma=x,y,z} \nu_\sigma (r_\sigma - Z_{i\sigma})^2\right\}(a_i\chi_\uparrow + b_i\chi_\downarrow)\eta_i. \tag{3}$$

Here, the isospin part η_i is fixed to either a proton or neutron. The Gaussian widths (ν_x, ν_y, ν_z), centroids $Z_{i\sigma}$, and spin directions a_i and b_i are the parameters of the model wave function (2) and are determined by the frictional cooling method, which minimizes the sum of the Hamiltonian and constraint potential,

$$E(\beta) = \frac{\langle \Phi^{\pi}|\hat{H}|\Phi^{\pi}\rangle}{\langle \Phi^{\pi}|\Phi^{\pi}\rangle} + v_\beta(\langle\beta\rangle - \beta)^2. \tag{4}$$

In this case, a sufficiently large value of the constraint potential strength v_β is selected to ensure that the quadrupole deformation parameter $\langle\beta\rangle$ [21] of the model wave function is equal to the input value β. Further, we obtain the optimized wave function $\Phi^{\pi}(\beta)$, which has the minimum energy for each given value of β.

After the energy variation, the optimized wave functions are projected to the eigenstate of the angular momentum,

$$\Phi^{J\pi}_{MK}(\beta) = \frac{2J+1}{8\pi^2}\int d\Omega\, D^{J\,*}_{MK}(\Omega)\hat{R}(\Omega)\Phi^{\pi}(\beta), \tag{5}$$

Downloaded from https://academic.oup.com/ptep/article/2022/11/113D01/6798384 by DESY-Zentralbibliothek user on 26 December 2022

where $D^J_{MK}(\Omega)$ and $\hat{R}(\Omega)$ denote Wigner's D-function and the rotation operator, respectively. Then, the projected wave functions that have different values of the deformation parameter β are superposed as

$$\Psi^{J\pi}_{\alpha} = \sum_{iK} g_{iK,\alpha} \Phi^{J\pi}_{MK}(\beta_i). \tag{6}$$

This is the wave function of the generator coordinate method (GCM) [22], where the deformation parameter β is employed as the generator coordinate (6). This GCM wave function can approximately describe the bound state as well as the unbound state with a bound-state approximation. The coefficients $g_{jK',\alpha}$ and the eigenenergy E_α are determined by solving the Hill–Wheeler equation [22]:

$$\sum_{jK'} (H_{iKjK'} - E_\alpha N_{iKjK'}) g_{jK',\alpha} = 0, \tag{7}$$

$$H_{iKjK'} = \left\langle \Phi^{J\pi}_{MK}(\beta_i) | \hat{H} | \Phi^{J\pi}_{MK'}(\beta_j) \right\rangle, \tag{8}$$

$$N_{iKjK'} = \left\langle \Phi^{J\pi}_{MK}(\beta_i) | \Phi^{J\pi}_{MK'}(\beta_j) \right\rangle. \tag{9}$$

The GCM wave functions can be used to derive the properties of Be and B isotopes, such as the distribution radii and degree of clustering.

2.2. *Reduced width amplitude*

To evaluate the degree of clustering in Be and B isotopes, we calculate the reduced width amplitude (RWA), which is defined as the overlap between the A-body GCM wave function and the reference state composed of a cluster with a mass C_1 and a daughter nucleus with a mass $A - C_1$. Thus, the RWA is the probability amplitude of a cluster at a distance $r = a$ from the daughter nucleus,

$$\mathcal{Y}_{C_1}(a) = \sqrt{\binom{A}{C_1}} \left\langle \tfrac{\delta(r-a)}{ra} Y_{\ell=0}(\hat{\boldsymbol{r}}) [\Phi^{0+}_{C_1} \Phi^{J\pi}_{A-C_1}] | \Phi^{J\pi}_{A} \right\rangle, \tag{10}$$

where $\Phi^{0+}_{C_1}$ is the fully antisymmetrized wave function of the cluster C_1 with spin-parity 0^+; $\Phi^{J\pi}_{A-C_1}$ and $\Phi^{J\pi}_{A}$ are the fully antisymmetrized wave functions of the ground states of the daughter and mother nuclei. The spin-parity J^π is 0^+ and $3/2^-$ for the Be and B isotopes, respectively. In this study, we only consider the orbital angular momentum of the intercluster motion, i.e., $\ell = 0$. In the practical calculations, Eq. (10) was evaluated by using the Laplace expansion method [23].

The degree of clustering may be evaluated by the spectroscopic factor (S-factor), which is the squared integral of the RWA:

$$S(C_1) = \int_0^\infty da\, |a\mathcal{Y}_{C_1}(a)|^2. \tag{11}$$

Notably, $S(C_1)$ is not normalized to unity because of the antisymmetrized effects between the cluster $S(C_1)$ and the daughter nucleus.

We also calculate the root mean square (RMS) radius of the RWA between the cluster C_1 and the daughter nucleus, defined by

$$a_{\mathrm{rms}}(C_1) \equiv \left[\int_0^\infty da\, a^2 |a\mathcal{Y}_{C_1}(a)|^2 \Big/ \int_0^\infty da\, |a\mathcal{Y}_{C_1}(a)|^2 \right]^{1/2}, \tag{12}$$

Downloaded from https://academic.oup.com/ptep/article/2022/11/113D01/6798384 by DESY-Zentralbibliothek user on 26 December 2022

Table 1. Calculated quadrupole deformation parameter β; the RMS proton, neutron, and matter distribution radii of the Be isotopes (unit: fm); and the principal neutron quantum numbers N_n. The approximated shell model (SM) and molecular orbital (MO) configurations [30] are also listed.

	β	$\sqrt{\langle r_p^2 \rangle}$	$\sqrt{\langle r_n^2 \rangle}$	$\sqrt{\langle r_m^2 \rangle}$	N_n	SM	MO
^{10}Be	0.60	2.44	2.49	2.47	4.03	$0\hbar\omega$	π^2
^{12}Be	0.55	2.57	2.85	2.76	7.60	$2\hbar\omega$	$\pi^2\sigma^2$
^{14}Be	0.60	2.62	2.99	2.88	10.01	$0\hbar\omega$	$\pi^4\sigma^2$

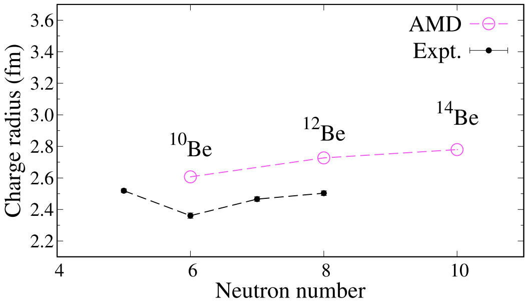

Fig. 1. Calculated RMS charge radii of the Be isotope ground states compared with those experimentally obtained from isotope shift measurements [16–18].

where an expectation value of the squared intercluster distance a is normalized by the S-factor, $S(C_1)$.

3. Results and discussion

3.1. *Structure of the ground states of Be isotopes*

Be isotopes are well known to have an enhanced two α-cluster core surrounded by valence neutrons; such cores have been studied using numerous cluster models [24–29]. In the molecular orbital model, the excess neutrons occupy the molecular orbitals and bond with the α particles [13–15,30]. ^{10}Be is dominated by the π^2 configuration, in which the two excess neutrons occupy the π orbitals corresponding to the spherical p orbitals in the limit of zero distance between the two α clusters. The two additional excess neutrons in ^{12}Be occupy the σ orbitals that correspond to the spherical sd-shell in the limit of zero distance between the two α clusters; further, the $\pi^2\sigma^2$ configuration is dominant in ^{12}Be. Similarly, the two additional excess neutrons in ^{14}Be occupy the π orbitals, and the $\pi^4\sigma^2$ configuration is dominant. It is considered that the σ-bond structure separates the α particles, while the π-bond structure brings them closer [26,29]. In an ordinary spherical shell model, ^{10}Be and ^{14}Be are dominated by the normal configuration (i.e., the $0\hbar\omega$ configuration). In contrast, ^{12}Be is dominated by the $2\hbar\omega$ configuration, in which two of the valence neutrons occupy the orbitals in the sd-shell beyond the $N = 8$ shell gap.

The ground-state properties of ^{10}Be, ^{12}Be, and ^{14}Be deduced by our calculations are summarized in Table 1. The point proton or charge distribution radii of the Be isotopes increase toward the neutron drip-line in accordance with the enhancement of clustering. In Fig. 1, both the observed and calculated RMS charge radii increase from ^{10}Be toward the neutron drip-line, although our calculations systematically overestimate the radii. This is because the Gogny interaction used in this study tends to overestimate the radii of the s-shell nuclei, in particular that of the α particle, which is an important ingredient in the clustered ground states of Be

Downloaded from https://academic.oup.com/ptep/article/2022/11/113D01/6798384 by DESY-Zentralbibliothek user on 26 December 2022

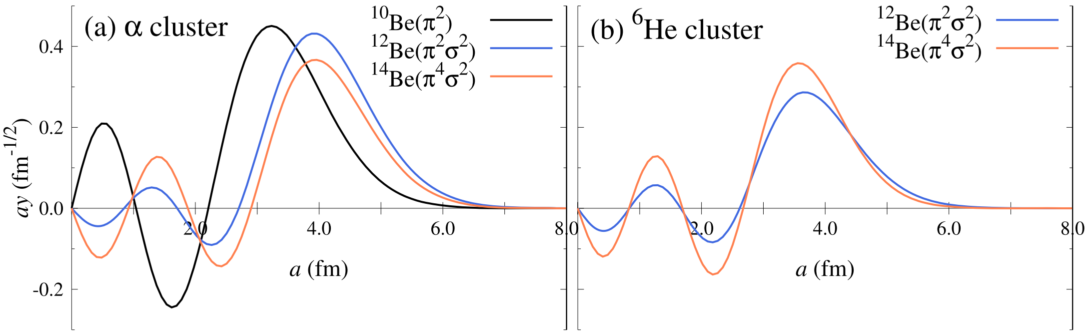

Fig. 2. The calculated α (a) and ^{6}He (b) RWAs of the Be isotopes with orbital angular momentum $\ell = 0$.

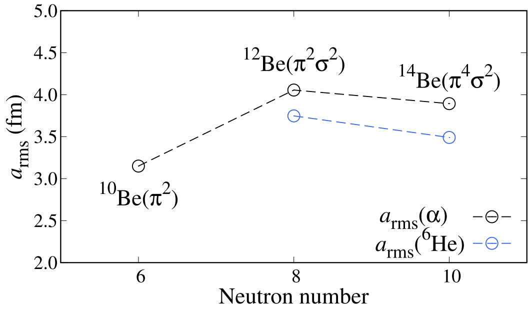

Fig. 3. Calculated RMS radii of the RWAs for α and ^{6}He clusters in the Be isotopes.

isotopes. The calculated RMS neutron and matter radii also show a similar trend. The large quadrupole deformation parameter β also supports the presence of two α-cluster cores with large intercluster distances. Moreover, the calculated principal neutron quantum numbers, N_n, of ^{10}Be and ^{14}Be are approximately 4 and 10, respectively, indicating the $0\hbar\omega$ configuration, whereas for ^{12}Be, $N_n \simeq 8$, which corresponds to the $2\hbar\omega$ configuration.

3.2. *Cluster formation in the ground states of Be isotopes*

Here, we discuss the enhancement of clustering in Be isotopes based on the calculated RWAs. Figure 2(a) shows the calculated α RWA of the ground state of ^{A}Be for the $|\alpha \otimes {}^{A-4}{\rm He}(0^+_1)\rangle$ channel. The amplitudes are suppressed and oscillate in the nuclear interior because of the Pauli exclusion principle. The effect of Pauli exclusion is approximately described by the Wildermuth–Tang rule [31], which asserts that the nodal quantum number n and orbital angular momentum ℓ of the RWA must satisfy the condition $2n + \ell \geq 4$ in ^{10}Be and $2n + \ell \geq 6$ in ^{12,14}Be. Thus, the α RWAs with $\ell = 0$ have two and three nodes in ^{10}Be and ^{12,14}Be, respectively. Note that the condition $2n + \ell \geq 6$ for ^{12}Be implies the dominance of the $2\hbar\omega$ configuration, i.e., the breaking of the $N = 8$ magic number. The amplitudes are peaked at the nuclear exterior ($r \gtrsim 3.0$ fm), indicating cluster formation at the nuclear surface. The peak position is more outward for ^{12,14}Be than for ^{10}Be, and this result is consistent with the enhanced cluster formation by the excess neutrons occupying the σ orbitals. This trend is also evident from the calculated RMS radius of the RWA, $a_{\rm rms}$, shown in Fig. 3. The $a_{\rm rms}(\alpha)$ of ^{12}Be is larger than that of ^{10}Be owing to the cluster development in ^{12}Be. Additionally, the $a_{\rm rms}(\alpha)$ of ^{14}Be is slightly shorter than that of ^{12}Be, because the two neutrons of ^{14}Be occupying the π orbitals attract the two α-cluster cores.

Downloaded from https://academic.oup.com/ptep/article/2022/11/113D01/6798384 by DESY-Zentralbibliothek user on 26 December 2022

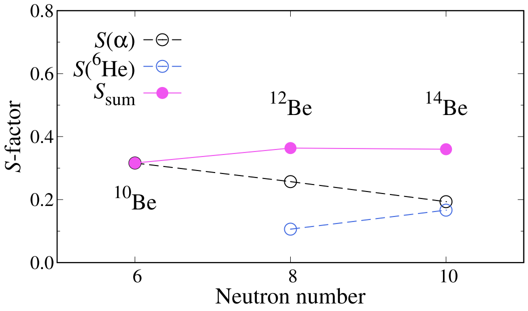

Fig. 4. Calculated α and ^{6}He S-factors and the sum of these S-factors as a function of the neutron number of the Be isotopes.

Table 2. Calculated deformation parameters β, γ; the RMS proton, neutron, and matter distribution radii; and the principal neutron quantum numbers N_n of the B isotopes. The γ values and radii are presented in units of degree and fm, respectively.

	β	γ	$\sqrt{\langle r_p^2 \rangle}$	$\sqrt{\langle r_n^2 \rangle}$	$\sqrt{\langle r_m^2 \rangle}$	N_n
^{11}B	0.45	59	2.45	2.49	2.47	4.03
^{13}B	0.30	6	2.47	2.56	2.52	6.04
^{15}B	0.50	0	2.61	2.87	2.79	10.00
^{17}B	0.55	9	2.66	3.02	2.92	14.01
^{19}B	0.45	60	2.69	3.12	3.01	18.01

However, the calculated S-factor for α clustering, shown in Fig. 4, contradicts the aforementioned analysis. The S-factor decreases as the neutron number increases, suggesting the suppression of α-cluster formation by the excess neutrons. The associated mechanism may be explained as follows: Because of the glue-like role played by the valence neutrons in ^{12}Be, this Be isotope has a mixing of $\alpha + {}^8$He and ^{6}He+^{6}He configurations. As a result, the $S(\alpha)$ of ^{12}Be becomes smaller than that of ^{10}Be, although the sum of $S(\alpha)$ and $S(^6\text{He})$ is larger than that of ^{10}Be. Similarly, ^{14}Be may be an admixture of the $\alpha + {}^{10}$He and ^{6}He+^{8}He configurations. To verify this hypothesis, the calculated ^{6}He RWAs of ^{12}Be and ^{14}Be are shown in Fig. 2(b). In both ^{12}Be and ^{14}Be, the peak height of the ^{6}He RWA is comparable to that of the α RWA, and the peak position slightly shifts inward, which is reflected by the RMS radii of the RWAs for the α and ^{6}He clusters shown in Fig. 3. Thus, the magnitude of $S(^6\text{He})$ is comparable with that of $S(\alpha)$. The sum of $S(\alpha)$ and $S(^6\text{He})$ (i.e., S_{sum}) does not decrease with increasing neutron number but increases slightly. Thus, taking into account the clustering of ^{6}He as well as α, it can be stated that Be isotopes have a well-developed cluster structure.

3.3. *Structure of ground states of B isotopes*

Although the structures of B isotopes have been theoretically studied by many authors [10–12,32–34], the physical quantities, which facilitate a direct analysis of clustering, have not been discussed. Here, we explain our calculated ground-state properties of B isotopes. Table 2 lists the calculated quadrupole deformation parameters β and γ, and the RMS proton, neutron, and matter distribution radii of the B isotopes. The principal neutron quantum numbers, N_n, are approximately 4, 6, 10, 14, and 18 for ^{11,13,15,17,19}B, respectively, indicating that all the B isotopes are dominated by the $0\hbar\omega$ configurations. The deformation parameters γ show that

Downloaded from https://academic.oup.com/ptep/article/2022/11/113D01/6798384 by DESY-Zentralbibliothek user on 26 December 2022

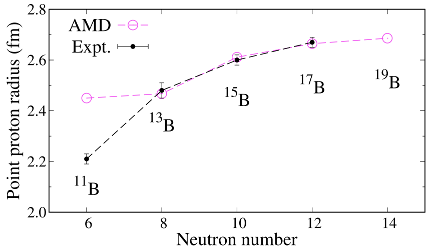

Fig. 5. Calculated RMS point proton radii of the B isotopes compared with the corresponding observed values [35,36].

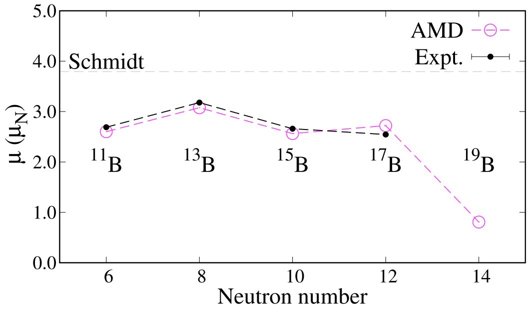

Fig. 6. Calculated magnetic moments μ of the B isotopes compared with the observed values [37–40]. The gray dashed line shows the Schmidt value for the $p_{3/2}$ proton.

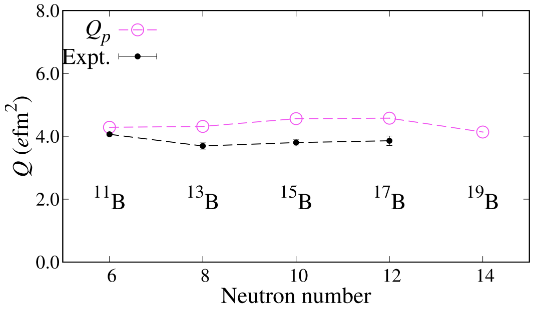

Fig. 7. Calculated electric quadrupole moments Q_p of the B isotopes compared with the observed values [41–43].

^{13}B, ^{15}B, and ^{17}B are prolately deformed, while ^{11}B and ^{19}B are oblately deformed. Remarkably, in the present calculations, ^{19}B is oblately deformed ($\gamma_{p,n} \approx 60^\circ$), while the spin-fixed AMD calculations [12] yielded a prolate deformation. This difference significantly affects the cluster formation probabilities as discussed later in this paper. Figure 5 shows the calculated RMS point proton radii, which are in reasonable agreement with the experimental values, except for ^{11}B. The magnetic moments μ and electric quadrupole moments Q_p of $^{11\text{–}17}$B shown in Figs. 6 and 7 are also in good agreement with the observed values and do not exhibit a strong dependence on the neutron number. Thus, the present calculation results successfully describe the ground states of B isotopes.

3.4. *Cluster formation in B isotopes*

In this subsection, we discuss the cluster formation in B isotopes based on the intrinsic density distributions, RWAs, radii of the RWAs, and S-factors.

Downloaded from https://academic.oup.com/ptep/article/2022/11/113D01/6798384 by DESY-Zentralbibliothek user on 26 December 2022

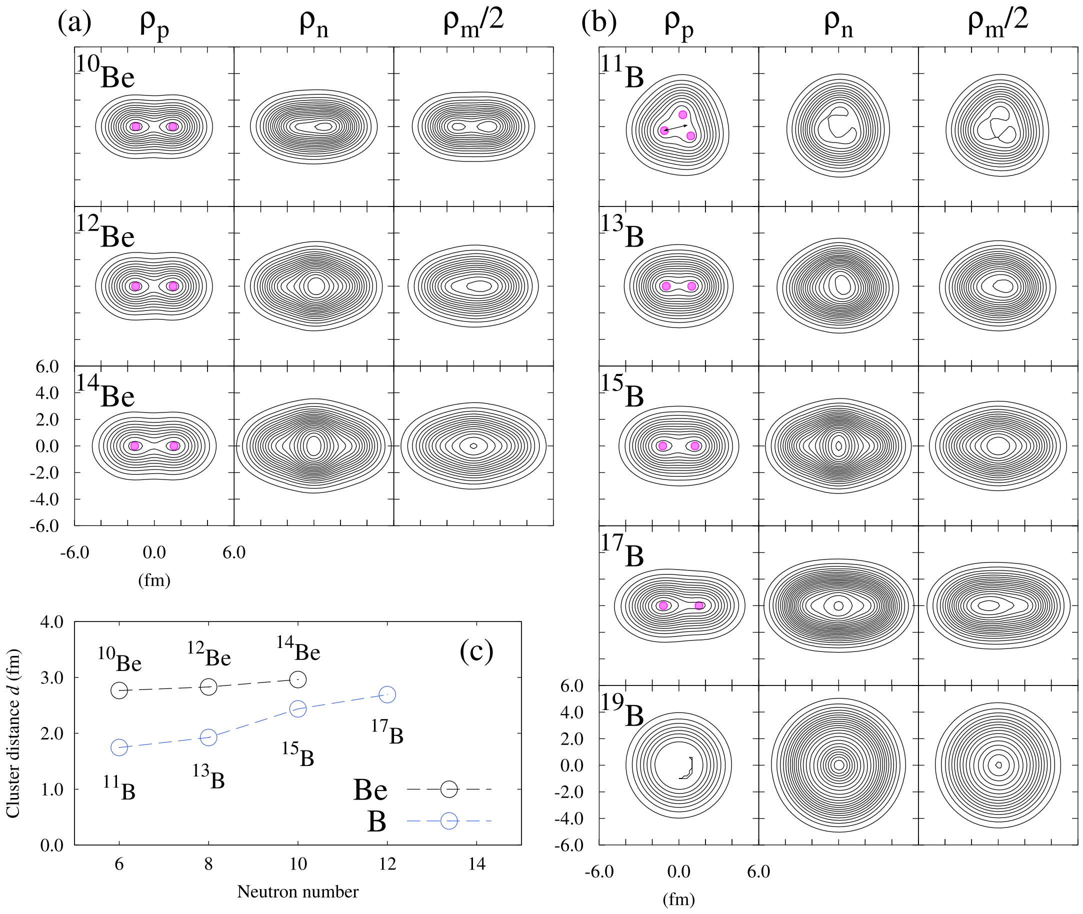

Fig. 8. Panels (a) and (b) show the proton, neutron, and matter intrinsic density of Be and B isotopes, respectively. The peak positions of the proton density distributions are marked by points and those distances are shown in panel (c). Note for ^{11}B that the largest distance between one peak and the mean position of the other peaks is adopted and shown as an arrow.

Cluster formation in B isotopes can be evaluated from Fig. 8, which shows the proton, neutron, and matter intrinsic density distributions of the Be and B isotopes. The peak positions of the proton density distributions are marked by points, and the distances *d* between them are shown in panel (c). All the Be isotopes exhibit a prolate shape, and the distance *d* increases as the neutron number increases, which is consistent with the growth of clustering toward the neutron drip-line. For the B isotopes, the *S*-factors are expected to be smaller than those of the Be isotopes, because the distance *d* is smaller than that of the Be isotopes. The *S*-factor increases as a function of the neutron number until ^{17}B. The isotope ^{19}B has an oblate shape and does not exhibit clustered structures. Thus, we expect that the clustering is enhanced until ^{17}B, but the corresponding *S*-factors are always smaller than those of the Be isotopes.

Next, we discuss the RWAs in the $|\alpha\otimes{}^{A-4}\mathrm{Li}(3/2_1^-)\rangle$ channel with $A = 11$, 13, and 15 as shown in Fig. 9(a). The RWAs of the B isotopes are peaked at the nuclear exterior and suppressed in the interior because of the Pauli exclusion satisfying the Wildermuth–Tang rule [31]. The peak height is much smaller than that of the Be isotopes, suggesting the presence of less developed clustered structures as expected. Similar to the case of Be and C isotopes [8], $S(\alpha)$ decreases as the neutron number increases as shown in Fig. 10 because of the excess neutrons, which cause

Downloaded from https://academic.oup.com/ptep/article/2022/11/113D01/6798384 by DESY-Zentralbibliothek user on 26 December 2022

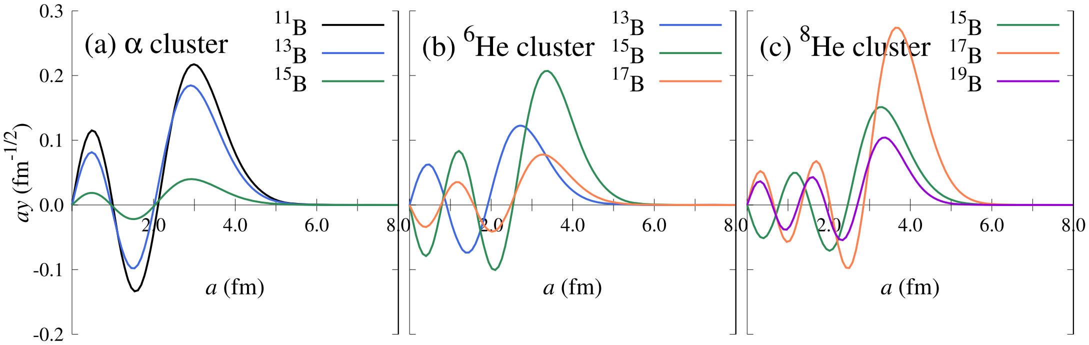

Fig. 9. Calculated α (a), ^{6}He (b), and ^{8}He (c) RWAs of the B isotopes with an orbital angular momentum of $\ell = 0$.

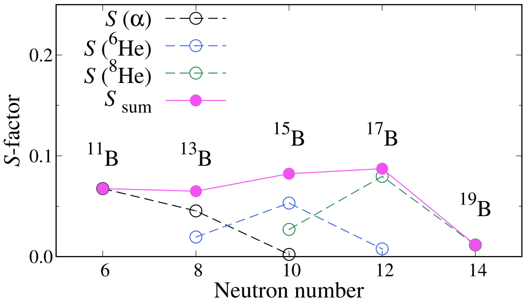

Fig. 10. Calculated α, ^{6}He, and ^{8}He S-factors and the sum of those S-factors as a function of the neutron number of the B isotopes.

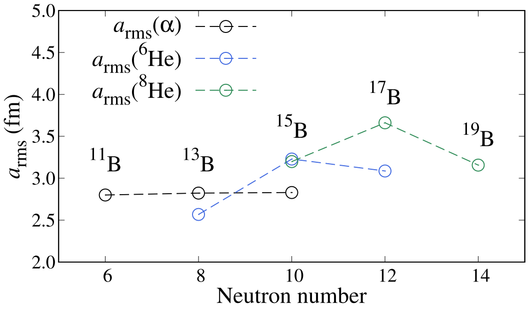

Fig. 11. Calculated RMS radii of the RWAs for α, ^{6}He, and ^{8}He clusters of the B isotopes.

the mixing of the α + ^{9}Li and ^{6}He+^{7}Li configurations in ^{13}B and that of the ^{6}He+^{9}Li and ^{8}He+^{7}Li configurations in ^{15}B. The calculated ^{6}He and ^{8}He RWAs are shown in Figs. 9(b) and (c), respectively. Evidently, in ^{13}B, the peak height of the ^{6}He RWA is comparable to that of the α RWA. In ^{15}B, the peak heights of the ^{6}He and ^{8}He RWAs are larger than that of α. Similarly, the excess neutrons in ^{17}B contribute to the formation of the ^{8}He+^{9}Li configuration. These features are reflected in the S-factors depicted in Fig. 10 as well as the radii of the RWAs shown in Fig. 11. Clearly, some of the α, ^{6}He, and ^{8}He cluster structures are enhanced in ^{11,13,15,17}B. In Fig. 10, $S_{\rm sum}$ shows the sum of $S(\alpha)$, $S(^6{\rm He})$, and $S(^8{\rm He})$ and is not hindered by the excess neutrons in the isotopes up to ^{17}B.

In ^{19}B, the corresponding RWA and S-factor indicate a less developed ^{8}He cluster structure, which is expected from the intrinsic densities. Therefore, the behavior of $S_{\rm sum}$ is consistent with the enhancement of clustering, determined from the intrinsic density distributions in Fig. 8.

Downloaded from https://academic.oup.com/ptep/article/2022/11/113D01/6798384 by DESY-Zentralbibliothek user on 26 December 2022

This figure indicates a certain amount of cluster development at S_{sum} values smaller than that of Be isotopes.

4. Summary

In this study, AMD calculations were performed that predicted the enhancement of α-cluster formation in Be and B isotopes as the neutron drip-line is approached, which is opposite to the experimental observations of Sn isotopes. Experimental investigation of the cluster formation based on the physical quantities that can directly probe the cluster structure is a considerable challenge. Thus, we theoretically evaluated the cluster formation in Be and B isotopes to clarify the possible clustering as the neutron drip-line is approached. We investigated the cluster formation probability at the nuclear surface by analyzing the ^{6}He and ^{8}He clusters that are expected to emerge because of the excess neutrons as well as the α clusters. The AMD framework successfully described the ground-state properties of both the Be and B isotope chains. We estimated the enhancement of clustering from the intrinsic density distributions in the Be and B isotopes as well as by using the molecular orbital model for the Be isotopes. Although the calculated α spectroscopic factors (i.e., $S(\alpha)$) show a negative correlation with the neutron number, the sum of $S(\alpha)$ and $S(^6\text{He})$ for the Be isotopes and that of $S(\alpha)$, $S(^6\text{He})$, and $S(^8\text{He})$ for the B isotopes are not being hindered as the neutron drip-line approaches, except for ^{19}B. This result is consistent with the enhancement of clustering estimated from the intrinsic density distributions. Thus, the results of this study reveal the possibility of cluster formation as the neutron drip-line is approached in Be and B isotopes. These results are based on the discussion, which explains the mechanism of cluster formation in Be isotopes and shows the consistency between the cluster distances of the intrinsic density distributions and cluster formations in B isotopes. Consequently, the results indicate that ^{6}He and ^{8}He clusters are formed along with α clusters owing to the excess neutrons surrounding the α-cluster cores.

Acknowledgements

This work was supported by JST SPRING, Grant Number JPMJSP2119, and JSPS KAKENHI Grant Nos. 21H00113 and 22H01214. We would like to thank Editage (www.editage.com) for English language editing.

Downloaded from https://academic.oup.com/ptep/article/2022/11/113D01/6798384 by DESY-Zentralbibliothek user on 26 December 2022

Appendix A. Principal neutron quantum number

The number operator $\hat{n}_\sigma = \hat{a}_\sigma \hat{a}_\sigma^\dagger$ is defined as

$$\hat{a}_\sigma = \sqrt{\nu_\sigma}\left(\hat{\sigma} + \frac{\hat{p}_\sigma}{2i\hbar\nu_\sigma}\right), \tag{A1}$$

$$\hat{a}_\sigma^\dagger = \sqrt{\nu_\sigma}\left(\hat{\sigma} - \frac{\hat{p}_\sigma}{2i\hbar\nu_\sigma}\right), \tag{A2}$$

where ν_σ is a Gaussian width of $\sigma = x, y, z$ direction and $\hat{p}_\sigma$ is a momentum operator. The principal neutron quantum number N_n is calculated using the number operator $\hat{n}_\sigma$, which is acted on the neutron part of the parity-projected wave function (2):

$$N_n = \sum_{i \in \text{neutron}} \sum_{\sigma = x,y,z} \langle \hat{n}_\sigma \rangle_i = \sum_{i \in \text{neutron}} \sum_{\sigma = x,y,z} \frac{\left\langle \Phi^\pi \middle| \hat{a}_{i,\sigma} \hat{a}_{i,\sigma}^\dagger \middle| \Phi^\pi \right\rangle}{\langle \Phi^\pi | \Phi^\pi \rangle}. \tag{A3}$$

References

[1] S. Typel, G. Röpke, T. Klähn, D. Blaschke, and H. H. Wolter, Phys. Rev. C **81**, 015803 (2010).
[2] K. Hagel et al., Phys. Rev. Lett. **108**, 062702 (2012).
[3] S. Typel, H. H. Wolter, G. Röpke, and D. Blaschke, Eur. Phys. J. A **50**, 1 (2014).
[4] Z.-W. Zhang and L.-W. Chen, Phys. Rev. C **95**, 064330 (2017).
[5] S. Typel, Phys. Rev. C **89**, 064321 (2014).
[6] K. Yoshida, Y. Chiba, M. Kimura, Y. Taniguchi, Y. Kanada-En'yo, and K. Ogata, Phys. Rev. C **100**, 044601 (2019).
[7] J. Tanaka et al., Science **371**, 260 (2021).
[8] Q. Zhao, Y. Suzuki, J. He, B. Zhou, and M. Kimura, Eur. Phys. J. A **57**, 1 (2021).
[9] H. Horiuchi, Y. Kanada-En'yo, and A. Ono, Z. Phys. A **349**, 279 (1994).
[10] Y. Kanada-En'yo and H. Horiuchi, Phys. Rev. C **52**, 647 (1995).
[11] H. Horiuchi and Y. Kanada-En'yo, Nucl. Phys. A **616**, 394 (1997).
[12] Y. Kanada-En'yo and H. Horiuchi, Prog. Theor. Phys. Suppl. **142**, 205 (2001).
[13] Y. Abe, J. Hiura, and H. Tanaka, Prog. Theor. Phys. **49**, 800 (1973).
[14] H. Furutani, H. Kanada, T. Kaneko, S. Nagata, H. Nishioka, S. Okabe, S. Saito, T. Sakuda, and M. Seya, Prog. Theor. Phys. Suppl. **68**, 193 (1980).
[15] M. Seya, M. Kohno, and S. Nagata, Prog. Theor. Phys. **65**, 204 (1981).
[16] W. Nörtershäuser et al., Phys. Rev. Lett. **102**, 062503 (2009).
[17] M. Žáková et al., J. Phys. G: Nucl. Part. Phys. **37**, 055107 (2010).
[18] A. Krieger et al., Phys. Rev. Lett. **108**, 142501 (2012).
[19] J. F. Berger, M. Girod, and D. Gogny, Comput. Phys. Commun., **63**, 365 (1991).
[20] M. Kimura, Phys. Rev. C **69**, 044319 (2004).
[21] M. Kimura, R. Yoshida, and M. Isaka, Prog. Theor. Phys. **127**, 287 (2012).
[22] D. L. Hill and J. A. Wheeler, Phys. Rev. **89**, 1102 (1953).
[23] Y. Chiba and M. Kimura, Prog. Theor. Exp. Phys. **2017**, 053D01 (2017).
[24] M. Seya, M. Kohno, and S. Nagata, Prog. Theor. Phys. **65**, 204 (1981).
[25] W. von Oertzen, Z. Phys. A **354**, 37–43 (1996).
[26] N. Itagaki and S. Okabe, Phys. Rev. C **61**, 044306 (2000).
[27] M. Ito, K. Kato, and K. Ikeda, Phys. Lett. B **588**, 43 (2004).
[28] Y. Kanada-En'yo, M. Kimura, and A. Ono, Prog. Theor. Exp. Phys. **2012**, 01A202 (2012).
[29] M. Kimura, T. Suhara, and Y. Kanada-En'yo, Eur. Phys. J. A **52**, 1 (2016).
[30] Y. Kanada-En'yo, Phys. Rev. C **85**, 044320 (2012).
[31] K. Wildermuth and Y. C. Tang, (Academic Press, New York, 1977, A Unified theory of the nucleus. [Monograph]).
[32] Y. Kanada-En'yo, Phys. Rev. C **91**, 014315 (2015).
[33] N. Imai et al., Phys. Lett. B **673**, 179 (2009).
[34] P. Arumugam, B. K. Sharma, S. K. Patra, and R. K. Gupta, Phys. Rev. C **71**, 064308 (2005).
[35] B. M. Barnett et al., Phys. Lett. B **97**, 45 (1980).
[36] A. Estradé et al., Phys. Rev. Lett. **113**, 132501 (2014).
[37] J. H. Kelley, E. Kwan, J. E. Purcell, C. G. Sheu, and H. R. Weller, Nucl. Phys. A **880**, 88 (2012).
[38] F. Ajzenberg-Selove, Nucl. Phys. A **523**, 1 (1991).
[39] H. Okuno et al., Phys. Lett. B, **354**, 41 (1995).
[40] H. Ueno et al., Phys. Rev. C **53**, 2142 (1996).
[41] F. Ajzenberg-Selove, Nucl. Phys. A **506**, 1 (1990).
[42] H. Izumi et al., Phys. Lett. B **366**, 51 (1996).
[43] H. Ogawa et al., Phys. Rev. C **67**, 064308 (2003).

Downloaded from https://academic.oup.com/ptep/article/2022/11/113D01/6798384 by DESY-Zentralbibliothek user on 26 December 2022